JCTC Journal of Chemical Theory and Computation

Article

pubs.acs.org/JCTC

Electronic Excited States in Amorphous MEH-PPV Polymers from Large-Scale First Principles Calculations

Haibo Ma*

Key Laboratory of Mesoscopic Chemistry of MOE, School of Chemistry and Chemical Engineering, Institute of Theoretical and Computational Chemistry, Nanjing University, Nanjing 210093, China

Ting Qin and Alessandro Troisi*

Department of Chemistry and Centre of Scientific Computing, University of Warwick, Coventry CV4 7AL, United Kingdom

ABSTRACT: The electronic excited states of amorphous polymeric semiconductor MEH-PPV are investigated by first principles quantum chemical calculations based on trajectories from classical molecular dynamics simulations. We inferred an average conjugation length of ∼5−7 monomers for lowest vertical excitations of amorphous MEH-PPV at room temperature and verified that the normal definition of a chromophore in a polymer based on purely geometric "conjugation breaks" is not always valid in amorphous polymers and a rigorous definition can be only on the basis of the evaluation of the polymer excited state wave function. The charge transfer character is observed to be nearly invariant for all excited states in low energy window while the exciton delocalization extent is found to increase with energy. The interchain excitonic couplings for amorphous MEH-PPV are shown to be usually smaller than 10 meV suggesting that the transport mechanism across chain can be described by incoherent hopping. All these observations about the energetic and spatial distribution of the excitons in polymer as well as their couplings provide important qualitative insights and useful quantitative information for constructing a realistic model for exciton migration dynamics in amorphous polymer materials.

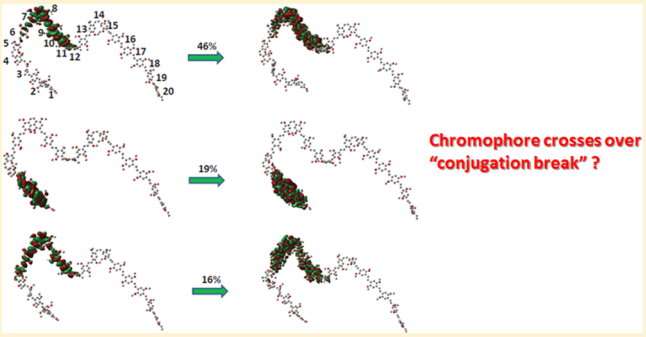

I. INTRODUCTION

Low-cost and flexible conjugated polymers are excellent candidates for the applications in electronics and photovoltaics.[1−3] Recently, the power conversion efficiency of polymer-based solar cells have been reported to exceed 10%[4,5] and a number of polymers were found to display charge mobility above 1 $cm^2\ V^{-1}\ s^{-1}$.[6−8] It is obvious that the energy and charge transport properties of such polymer-based systems depends on whether their morphologies are semicrystalline or amorphous. Although it is generally considered that semicrystalline conjugated polymers, which have better conjugation behavior with increased local order, will exhibit faster charge and energy migration, several amorphous polymers have been recently used in high efficiency solar cells.[9−13] This indicates that our fundamental understandings of the relationship between the conformations of the polymer chains and the ground and excited electronic structures as well as the photovoltaic conversion mechanism in such amorphous polymer-based systems still need great improvements.

Nowadays, most of the model interpretations of the static properties and the dynamic behavior of the excited states in conjugated polymers are based on the key concept of "exciton" (using solid state physics language) or "chromophore" (in chemical language).[14−25] From a physical point of view, the exciton is a bound electron−hole excited state, which is a linear combination of many electron−hole excitation pairs. Obviously, quantitative results of any exciton models should be much dependent on how the exciton states are distributed, in energy and space, which is still not very clear at the moment. For example, the common definition of a chromophore as a region of a polymer chain separated by geometric "conjugation breaks",[26] described by some minimum threshold in the π-orbital overlap, is surprisingly not valid for the electronic excitations in amorphous polymers, possibly because of the multiple coexisting mechanisms for excitonic couplings including dipole−dipole and through-bond superexchange interactions.[24] The interpretation of the experiment is further complicated by the fact that the conjugation length of the polymers affecting the delocalization extent of the excitons is known to be quite sensitive to the environmental factors.[27,28] Therefore, model studies without realistic parameters for different chemical structures under certain external conditions have difficulties in giving quantitatively correct pictures for the related optoelectronic processes in polymer-based materials, especially in consideration of the high variability for the

Received: December 13, 2013
Published: January 31, 2014

   dx.doi.org/10.1021/ct4010799 | J. Chem. Theory Comput. 2014, 10, 1272−1282

chemical compositions and local morphologies of polymers. Further quantitative characterizations of the nature and properties of the excitons and their dynamics are accordingly highly desired. Going beyond phenomenological models will help building structure−property relationship for chemically relevant polymers, but it requires the construction of an atomistic model for polymer-based systems and the calculation of its electronic structures of excited states, both of which are quite challenging even with state-of-art computational methodologies due to the large size of amorphous polymer systems.

Up to now, most of computational papers in the optoelectronic polymer field were only focusing on either the conformation information by simulations with classical force fields[29,30] or the electronic structure of an isolated polymer chain by quantum chemical calculations.[31−36] Very recently, research works aiming at the combination of these two aspects were reported. For example, Wang et al.[37,38] built microscopic models for PhEtTh and P3HT by classical molecular dynamics (MD) simulations and then studied the disorder effect on the electronic couplings and density of states as well as wave function localization in conjugated polymers. The similar strategy was also employed by Poelking et al.[39] to evaluate the charge-transport parameters for crystalline PBTTT by semiempirical Zerner's intermediate neglect of differential overlap (ZINDO) method.[40,41] Two of our authors (A.T. and T.Q.) and their co-workers also established the relationships between the morphologies and the electronic structures of crystalline P3HT and amorphous MEH-PPV.[42,43] However, such kind of combined morphology-electronic structure study for the excited states of polymer systems is still quite rare due to the difficulties in large-scale excited state calculations, especially from first principles methods, although it is vital for understanding and modeling photovoltaics or electroluminescence in polymer-based materials. In a seminal paper of this kind, Barford et al.[44,45] studied the excited state properties in a realistic polymer chain using the semiempirical Pariser−Parr−Pople model based on the atomic models for poly(paraphenylene) and P3HT from random statistical generations or classical MD simulations. They introduced an important concept of "local exciton ground states (LEGSs)"[44−47] as a special kind of exciton in conducting polymers to provide more rigorous definitions for absorption "chromophore" in polymers and the basis for modeling of exciton dynamics. In another seminal paper of this kind, the Beljonne group further explored the influence of bulk environment on the lowest excitations in model chains of MEH-PPV using the ZINDO Hamiltonian.[48] They found that the conjugation length for both isolated chains and the bulk material are around eight monomers and that the local fluctuations may increase the planar ratio of the polymer chain and accordingly induce red shift for absorption spectra. Their "bulk" MEH-PPV system was limited to only three 10-monomer chains, possibly too "small" to correctly represent the amorphous morphology and evaluate the energetic and spatial distribution of the excitons. Moreover, it will be desirable to consider calculations beyond the single configuration interaction (CIS) scheme with ZINDO Hamiltonian, which have the well-known deficiency of overestimating the delocalization of the excited states like transition dipole moments in π-conjugated systems[49,50] due to the insufficient treatment of electron correlations at CIS level.

In this paper, we will focus on one of the most widely studied prototypical amorphous polymers, MEH-PPV (see Figure 1). The simpler PPV chain (without solubilizing group) has been

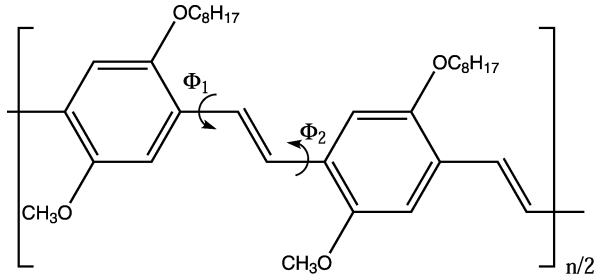

Figure 1. Molecular structure of polymer MEH-PPV (poly[2-methoxy-5-(2-ethylhexyloxy)-1,4-phenylenevinylene]).

for many years the test-bed for many theories of the excited states in organic polymer. Burghardt's group[35] and Nakatsuji's group[36] investigated the vertical excitations and torsional potentials of single PPV oligomer chain with high-level ab initio calculations and Tretiak's group[31,32] studied the localization of electronic excitations along PPV chains as a function of geometric distortion and polarization and the dependence of the results on the density functional used in the calculations. Nonadiabatic simulations of the excited chain dynamics for PPV or MEH-PPV including dynamical localization, exciton diffusion, and exciton dissociation were also performed by several groups[22−24,51−54] within semiempirical or empirical quantum chemical Hamiltonians. However, large-scale first principles excited state calculations based on realistic bulk models, which can give quantitative descriptions for excitons in conjugated polymer materials, are still absent for MEH-PPV (or any other polymer). Therefore, we will attempt such a theoretical work by performing large-scale first principles quantum chemical calculations with the time-dependent density functional theory (TDDFT)[55,56] for their electronic excited states based on reasonable atomistic models of amorphous system from MD simulations. Our main goal in this paper is to provide rigorous, microscopic information on the electronic excited states of polymer chains such as energetic distribution, spatial delocalization, charge-transfer character, and interchain excitonic couplings as well as their relationships with the amorphous conformations.

II. METHODS

Our electronic excited state calculations are based on trajectories generated by MD simulations of large-scale amorphous MEH-PPV model systems described in detail in ref 43. Two different systems composed of sixteen 20-monomer chains and sixteen 40-monomer chains each were studied at 1 atm and 300 K, and we refer to these models as m20 and m40 in the rest of this paper. The simulations were performed with modified potential in OPLS form[57] through conversion from MM3[58] force field by Rao's procedure[59,60] for the purpose of better describing the C−C bonds in large π-conjugated systems. More technical details about the simulation and the structural analysis of the results can be found in ref 43. For both m20 and m40, trajectories of 200 ns are available. Because it was found that the structural changes of MEH-PPV chains are very slow,[43] we only considered the 16 chains in a single snapshot at 200 ns for each system for the greatest part of our discussion but in the Results section, we will also consider the change of the excited states at for different snapshots of the trajectory.

In order to make the electronic excited state calculation costs affordable, we made the same simplifications proposed for the ground state electronic structure calculation in ref 43. First, the

side group $-OC_8H_{17}$ of each chain is replaced by the $-OCH_3$ group in order to speed up the calculation without altering the nature of frontier orbitals. Second, we suppose that the excitonic couplings of an individual chain with its surrounding chains are relatively small, an assumption that will be explicitly verified below, and we therefore calculate the electronic structure of each individual chain separately.

TDDFT calculations with long-range corrected ωB97X-D functional[61] and 6-31g* basis set for m20 (3-21g for m40) were implemented to calculate the lowest five singlet excited states for m20 (only lowest three states for m40 due to the limitation of our computational power). The impact of the reduced basis set and the number of electronic states included in the calculation is discussed in the Results section. Benchmark comparisons of TDDFT calculations with other popular functionals such as B3LYP,[62−64] CAM-B3LYP,[65] and M06-2X[66] and different basis sets as well as CIS calculations with the semiempirical ZINDO Hamiltonian[40,41] were also performed. To reproduce the electrostatic environment of each polymer chain, we used the electronic polarization embedding scheme,[67] by which the polarization of the QM subsystem by the surrounding charges residing on the MM atoms of the neighbor chains can be incorporated. This polarization is described by renormalizing the one-electron part of the effective Hamiltonian for the QM subsystem, allowing polarization of the QM wave function by the MM charges. Many recent studies such as the GW work by Neaton et al.[68] and the DFT work by Refaely-Abramson et al.[69] have also shown that including an effective dielectric environment into a first principles framework is indeed sufficient for polarization-induced renormalization. The background point charges were added in the atom positions close to the polymer chain of interest but belonging to other chains. The values of the point charges were the same used for the force field (optimized to reproduce the short-range electrostatic interaction). To avoid including an unbalanced number of point charges, the monomers of the surrounding chains within 10 Å from any atoms on the chain are identified first. The point charges for all atoms on these monomers (including the full side chains) are then added.

All the quantum chemical calculations in this work were performed with *Gaussian09* program package.[70]

To simulate the electronic absorption, we calculate the absorption intensity of the ith chain as

$$I_i(E) = \sum_n f_{0n}(i)\delta(E - E_i(n)) \tag{1}$$

where $f_{0n}(i)$ is the oscillator strength for the transition between the ground state and the nth excited state for the ith chain and $E_i(n)$ is the corresponding transition energy. The Dirac delta function $\delta(E - E_i(n))$ was approximated by a normalized Gaussian of standard deviation σ = 0.05 eV. The bulk absorption intensity of the MEH-PPV system is then calculated as

$$I_b(E) = \sum_{i=1}^{N} I_i(E)/N \tag{2}$$

where N is the total number of the chains.

In order to evaluate the contributions from different monomer units, we follow ref 48 to partition the wave function for the nth excited state S_n in the form of single particle excitations into local excitation configurations $|\psi_k\rangle$ and charge-transfer ones $|\psi_{k,l}\rangle$ (where k and l denote different monomer units)

$$|\Psi(n)\rangle = \sum_k c_k(n)|\psi_k\rangle + \sum_k \sum_{l\neq k} c_{k\to l}(n)|\psi_{k,l}\rangle \tag{3}$$

One may then calculate the overall contribution from the monomer k to the nth excited state as

$$b_k(n)^2 = c_k(n)^2 + \sum_{l\neq k} \frac{c_{k\to l}(n)^2}{2} \tag{4}$$

and the participation ratio (PR) for the excited state S_n can then be defined by

$$PR(n) = \frac{\sum_k b_k(n)^2}{\sum_k b_k(n)^4} \tag{5}$$

to describe the delocalization extent of various electronic excitations.

For the purpose of quantifying the charge transfer (CT) character of excited states, we define the electron−hole separation distance for nth excited state as

$$d_{e-h}(n) = \sqrt{\sum_m \lambda_m(n)|\mathbf{R}_m^o(n) - \mathbf{R}_m^v(n)|^2} \tag{6}$$

where $\lambda_m(n)$ is the eigenvalue of $T^\dagger T$ or $TT^\dagger$ (T is the transition density matrix between the ground state and nth excited state) and $\mathbf{R}_m^o(n)$ and $\mathbf{R}_m^v(n)$ are the centroid positions of corresponding occupied and virtual natural transition orbital (NTOs).[71] $\mathbf{R}_m^o(n)$ and $\mathbf{R}_m^v(n)$ can be calculated by $\mathbf{R}_m = \sum_i \mathbf{r}_i P_i^{(m)}$ where $\mathbf{r}_i$ is the coordinate of ith atom and $P_i^{(m)}$ is the weight of NTO m on a given atom i by

$$P_i^{(m)} = \sum_{s\in \text{atom } i; t\in \text{all atoms}} C_s^{(m)} S_{st} C_t^{(m)} \tag{7}$$

in which $C_s^{(m)}$ denotes the coefficient of atomic orbital s for NTO m and S_{st} is the overlap matrix of the basis set.

To evaluate the excitonic coupling $J_{mn}^{\alpha\beta}$ between the exciton α in chain m and the exciton β in chain n ($n \neq m$), we used the distributed monopole approximation[72] expressed as a Coulomb interaction term:

$$J_{mn}^{\alpha\beta} = \frac{1}{4\pi\varepsilon_0\varepsilon_r} \sum_{i\in m} \sum_{j\in n} \frac{q_i^t(\alpha) q_j^t(\beta)}{|\mathbf{r}_i - \mathbf{r}_j|} \tag{8}$$

where ε_0 is the vacuum permittivity and $q_i^t(\alpha)$ denotes the atomic transition charges at atom i between the ground state and the α excited state of chain m. We adopted a widely used value of 3 for the relative permittivity ε_r of MEH-PPV.[73]

III. RESULTS

A. Effects of DFT Functional, Basis Set, and Background Charge. To evaluate the effects of chosen DFT functionals and basis set as well as the background charges on the computational results of electronic excitations of amorphous MEH-PPV system, we first chose three representative chains in the m20 system at 200 ns to make preliminary comparisons. Figure 2 illustrates the absorption spectra by TDDFT calculations with the popular hybrid functional B3LYP[62−64] and some newly developed hybrid meta functional M06-2X[66] as well as long-range corrected functionals including CAM-B3LYP[65] and ωB97X-D.[61] It is shown that B3LYP

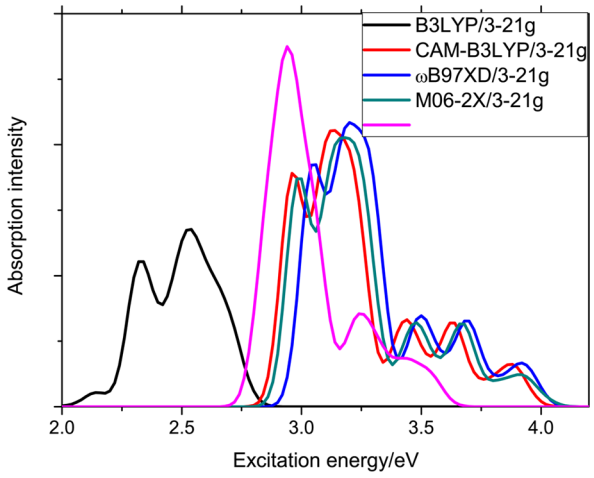

Figure 2. Calculated electronic absorption spectra for three representative chains of the m20 system at 200 ns by semiempirical ZINDO calculations and TDDFT calculations with different exchange-correlation functionals. (Five lowest singlet excitations were considered in the calculation of each chain.)

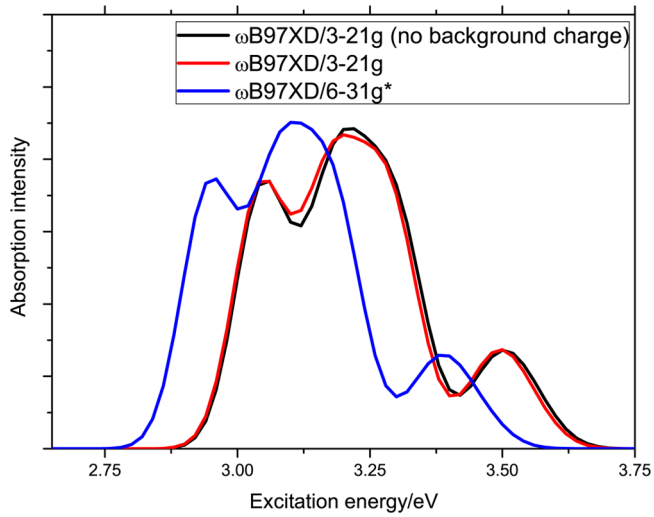

Figure 3. Calculated electronic absorption spectra for three representative chains of the m20 system at 200 ns by TDDFT calculations with different basis sets and with/without background charges. (Five lowest singlet excitations were considered in the calculation of each chain.)

underestimated the excitation energy remarkably compared with other functionals. This is not surprising because it is well-known that the standard hybrid exchange-correlation functionals underestimate the excitation energies for Rydberg states and charge-transfer states as well as $\pi \rightarrow \pi^*$ excitations in extended conjugated systems, because they do not exhibit the correct $1/r$ asymptotic behavior but decay too rapidly.[74] Such drawbacks can be (partly) overcome by the recent developments of long-range corrected exchange-correlation density functionals such as CAM-B3LYP and ωB97X-D. The M06-2X functional is a high-nonlocality functional with double the amount of nonlocal exchange (2X), and accordingly, it is also shown to be capable of improving the description for valence excitations in π-conjugated systems.[66,74] However, it is also worth being noticed that of the three improved functionals (CAM-B3LYP, ωB97X-D, and M06-2X), only ωB97X-D has a true $1/r$ asymptotic behavior. One may clearly see from Figure 2 that the difference among the results by these three improved functionals (CAM-B3LYP, ωB97X-D, and M06-2X) is quite small; therefore, we will adopt ωB97X-D for our all other TDDFT calculations. In Figure 2, we also illustrate the results by the CIS calculation within semiempirical ZINDO model, which is widely used for current electronic excited state studies of large molecular or polymer system. Although ZINDO predicts similar lowest excitation peak position here, the intensity and the properties of other higher peaks are quite different from first principles TDDFT calculations. Also considering that there have been many works reporting ZINDO's overestimating the delocalization of the excited states such as transition dipole moments in π-conjugated systems[49,50] due to the insufficient treatment of electron correlations at CIS level, we have to mention that such semiempirical calculations for excited state studies of conjugated polymeric systems should be used very carefully.

Figure 3 shows the calculated absorption spectra for selected chains with 3-21g and 6-31g* basis sets and with/without background charges. It is generally considered that, in contrast to the ground state calculation, a polarized and diffused basis set is necessary for accurate calculations of excited states. From Figure 3, one may clearly find that the spectra shapes by the two basis sets are quite similar to each other and there is only a pronounced red-shift of ∼0.12 eV when changing from 3-21g basis set to the larger 6-31g* basis set. We should note that our determined excitation energies for lowest absorption peaks (∼2.91 and 3.03 eV by 6-31g* and 3-21g, respectively) are still much higher than the experimental values of 2.25 eV using metal/polymer/metal structures[27] or 2.50 eV in methyltetrahydrofuran (MeTHF) solution at room temperature.[28] However, such discrepancy can be expected to reduce by further enlarging the basis set in quantum chemical calculations. Meanwhile, the similarity between the shapes of the absorption spectra computed with the 6-31g* and 3-21g basis set may imply that the economical basis set retains good quantitative information on the excited states and absorption intensity. Because the absorption spectra in Figure 3 is just an averaged result for three testing chains, we are not sure whether the high similarity of the spectra for the two basis set comes from the good correlation between the 3-21g calculations and 6-31g* calculations or only an averaging effect. Therefore, we plotted the calculated excitation energy and transition dipole moment values for the lowest 5 states of 16 individual chains with 6-31g* basis set against those by 3-21g basis set in Figure 4. Figure 4 shows surprisingly excellent linear relationships between the 6-31g* values and 3-21g results, implying that both basis sets can give very similar descriptions for the essential features of the valence excitations in conjugated polymers, at least the lowest ones. The slope of 1.0067 ± 0.0034 (1.0419 ± 0.0081) suggests errors less than 1% (5%) in the relative energy levels (transition dipole moments) and the intercept of −0.121 eV (−0.310 au) quantifies accurately the modest difference between basis sets. We checked the residual values (the differences between the observed value of the dependent variable and the predicted value) and found them to be distributed with variance 0.02 eV and 5 au for the transition energy and transition dipole moment, respectively. This indicates that electronic structure calculations with a basis set at the level similar to 3-21g or 6-31g* can give comparable results for the excited states of large polymer systems and, accordingly, they are useful for large-scale studies. For this

dx.doi.org/10.1021/ct4010799 | J. Chem. Theory Comput. 2014, 10, 1272−1282

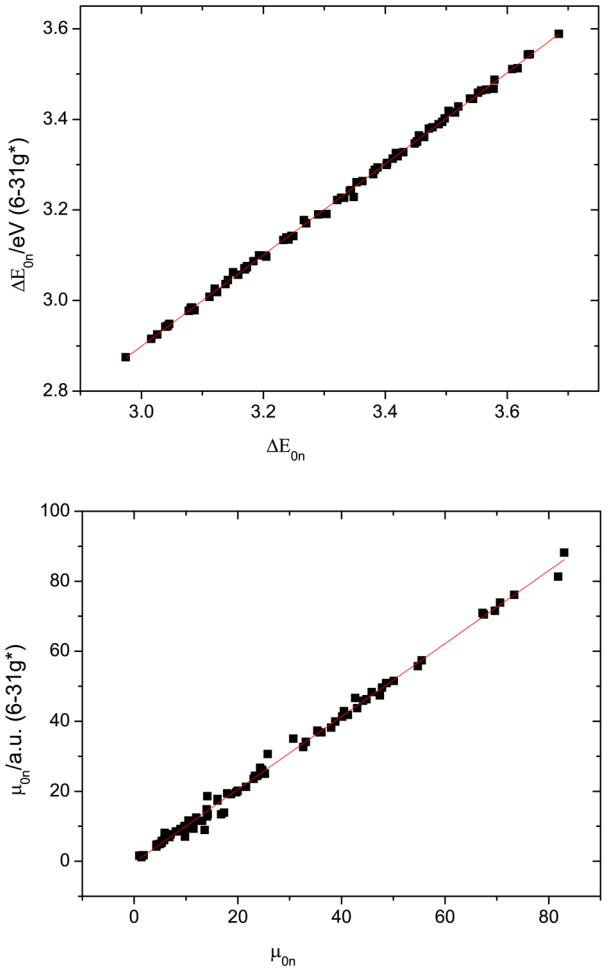

Figure 4. Correlation between excitation energy and transition dipole moment values obtained by ωB97X-D/3-21g and those by ωB97X-D/6-31g* for 16 individual chains of the m20 system at 200 ns. (Linear fittings give $\Delta E_{0n}(6-31g^*) = a + b \times \Delta E_{0n}(3-21g)$ with slope b = 1.0067 (standard error σ_b = 0.0034) and intercept a = −0.121 eV (σ_a = 0.011), and $\mu_{0n}(6-31g^*) = c + d \times \mu_{0n}(3-21g)$ with slope d = 1.0419 (standard error σ_d = 0.0081) and intercept c = −0.310 au (σ_c = 0.271).)

reason and also in consideration of the limitation of our current computational resources, we will adopt 6-31g* for the m20 system and 3-21g for the m40 system in our following systematic large-scale TDDFT calculations. The small 3-21g basis set works surprisingly well here, possibly because of some error cancelation in the calculation of the occupied and virtual orbital energy and because of *d* orbitals' small contribution to $\pi \rightarrow \pi^*$ excitations. Figure 3 also shows that the absorption shape does not change much when the background point charges are removed away. This implies that the electrostatic influence of other chains on the electronic excited states of one chain is quite small in this system and could be neglected.

B. Spatial Distribution of the Exciton and the Conformation−Electronic Structure Relationship. To illustrate the spatial distribution of the excitons, we plotted the mapping of the electronic transition density onto the monomers (see eq 4) of three representative chains of m20 system at 200 ns in Figure 5. Interestingly, we found in chain 6 that the lowest energy excitons tend to be of similar size and localized in some specific regions with very small spatial overlap between them. It is not always true that the lowest excitons are nonoverlapping as we have found in chains 1 and 11, which display more delocalized S_2−S_5 states, suggesting that a more rigorous analysis of the correlation between structure and delocalization is needed.

We used the folding and nonplanarity parameters[43] to characterize the defects in disordered systems. Looking at the chain folding sketch in Figure 6, one can use the distance *d* between the two carbon atoms in consecutive aromatic rings separated by a vinylene unit (labeled as "1" and "2" in Figure 6) to evaluate the folding defect's existence. The equilibrium value for such distance is approximately 3.9 Å for the perfect planar conformation, and thus, one may use $\Delta_k^{(d)} = |d - 3.90|$ to quantify the chain folding degree of monomer *k*. Similarly, one can define a torsion angle displacement from planarity by $\Delta_k^{(\Phi)} = \min\{|\Phi|,|180° - \Phi|\}$, where Φ denotes the dihedral angle Φ_1 or Φ_2 in Figure 1. The nonplanarity degree of monomer *k* is then calculated by $\overline{\Delta}_k^{(\Phi)} = (\Delta_k^{(\Phi_1)} + \Delta_k^{(\Phi_2)})/2$.

Figure 7 shows $\overline{\Delta}_k^{(\Phi)}$ and $\overline{\Delta}_k^{(d)}$ for the three representative chains. Obviously, it is difficult to find any direct relationship between the geometric distortion and the wave function distribution from the correspondence between Figure 5 and Figure 7. This verified again that it is difficult to define a chromophore in amorphous polymers as a region of a polymer chain separated by geometric "conjugation breaks".[26] Because dipole−dipole excitonic couplings do not depend on the π-orbital overlap, the excitons may spread over defects. For example, from Figure 7, one may notice there is a strong folding around monomer 8 in chain 11, but we found S_2 can spread over this defect from Figure 5. We illustrated their natural transition orbital pairs for such a $S_0 \rightarrow S_2$ transition in the bottom panel of Figure 5. Although S_2 and S_3 in chain 11 may be considered as the positive and negative linear combinations of the fragment excitation in the left end (monomer 1−4) and the fragment excitation in the left-middle region (monomer 5−12) due to the weak couplings, the latter fragment excitation is clearly spreading over the folding defect around monomer 8. This is a strong evidence that the pure geometric definition of a chromophore may fail for the electronic excitations in amorphous polymers. Nevertheless, it is also worth noting that low energy excitons are not found in regions highly nonplanar and folded, such as in the region between monomer 14 and monomer 18 of chain 1, where the systems is effectively less conjugated. In general, if we only focus on lowest excitations (one to three for m20), they are typically localized nodelessly with very small overlaps with other lowest excitons. Sometimes, excitons fulfilling such characteristics are also termed as local exciton ground states (LEGSs)[44−47] for convenience. They are considered as the "chromophore" for absorption in low-energy windows and the final state following an exciton transfer process. They have also been used as a basis for more rigorous modeling of exciton dynamics.[22] Our results from first principles calculations confirm the existence of LEGSs, originally proposed based on empirical model calculations.[46,47] Several LEGSs will approximately span the entire chain together and the ability to define them rigorously from the electronic wave function may help constructing quantitative model for exciton transport via incoherent hopping between LEGSs.

One of the key issues for polymer research is to establish the relationship between the geometric disorders and the electronic structures. Although we have found it is difficult to build direct relationship between the geometric distortion and the electronic density distribution, we also noticed strong disorders

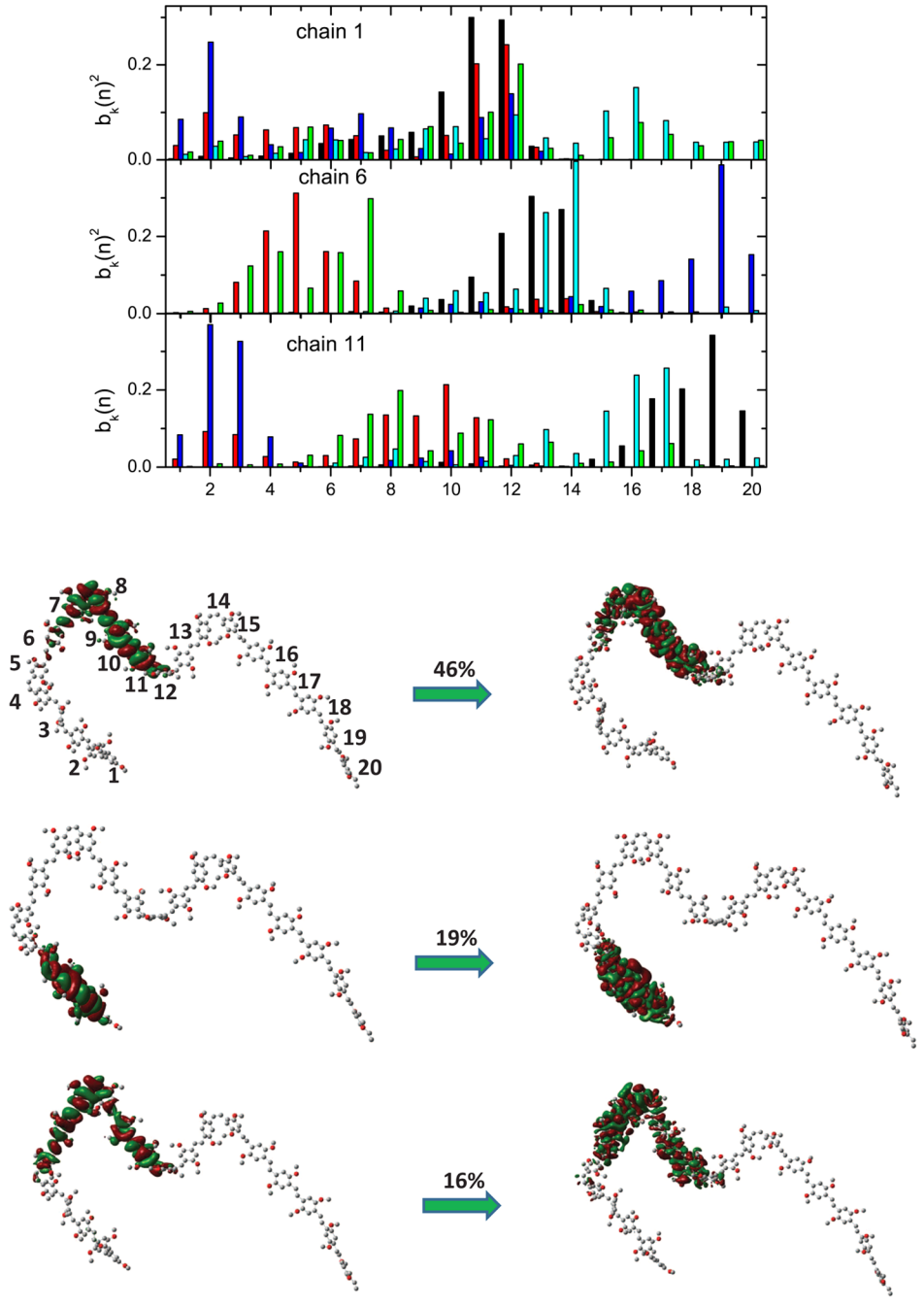

Figure 5. Mapping of the electronic transition density onto the monomers of three representative chains of m20 system at 200 ns (black, red, blue, cyan, and green colors are for S_1, S_2, S_3, S_4, and S_5, respectively) in the top panel and natural transition orbitals for $S_0 \rightarrow S_2$ of chain 11 in the bottom panel.

may disfavor the presence of a low energy exciton. To make our analysis more quantitative we define new parameters λ_f^{chain} and λ_p^{chain} to characterize the folding and nonplanarity of the whole single chains, using the parameters $\Delta_k^{(d)}$ and $\overline{\Delta}_k^{(\Phi)}$ defined above for the monomers:

$$\lambda_f^{chain} = \sum_{k=1}^{M} \Delta_k^{(d)}/M \tag{9}$$

$$\lambda_p^{chain} = \sum_{k=1}^{M} \overline{\Delta}_k^{(\Phi)}/M \tag{10}$$

where M is the number of monomers per chain. For the purpose of studying the correlation between these disorders and electronic transitions, we extended such analysis to the NTOs of electronic transitions by defining

$$\lambda_f^{S_0 \rightarrow S_n} = \sum_{k=1}^{M} \Delta_k^{(d)} P_k^{S_0 \rightarrow S_n} \tag{11}$$

and

$$\lambda_p^{S_0 \rightarrow S_n} = \sum_{k=1}^{M} \overline{\Delta}_k^{(\Phi)} P_k^{S_0 \rightarrow S_n} \tag{12}$$

dx.doi.org/10.1021/ct4010799 | J. Chem. Theory Comput. 2014, 10, 1272−1282

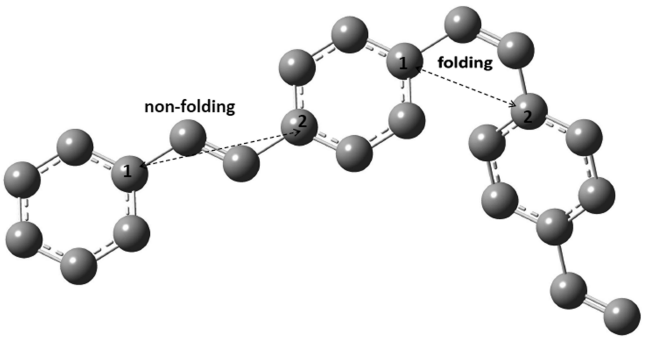

Figure 6. Sketch of chain folding with a MEH-PPV chain. (Only carbon atoms in the conjugated backbone were shown.)

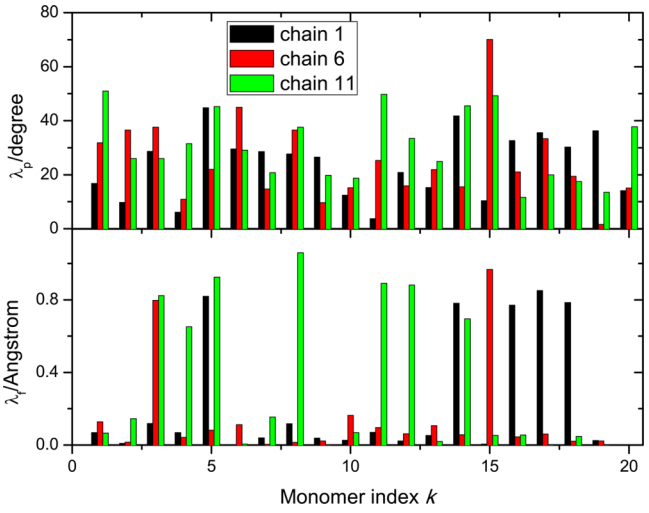

Figure 7. Nonplanarity and folding parameters for three representative chains of m20 system at 200 ns.

where $P_k^{S_0 \rightarrow S_n}$ is the weight of $S_0 \rightarrow S_n$ transition density on monomer k. $\lambda_{fk}^{S_0 \rightarrow S_n}$ or $\lambda_p^{S_0 \rightarrow S_n}$ are a measure of how folded or nonplanar are the chains in the region where exciton S_n is located. By comparing the distribution of these quantities with the distribution of λ_f^{chain} and λ_p^{chain}, we can establish if there is a correlation between the folding and nonplanarity and the most likely position of the low energy excitons. Figure 8 shows the histogram distribution of λ_f and λ_p the backbone of the chain and the transitions of $S_0 \rightarrow S_1$ and $S_0 \rightarrow S_5$ for m20 system at 200 ns. (We removed data for $S_0 \rightarrow S_2$ to $S_0 \rightarrow S_4$ in Figure 8 for a clearer illustration.) The statistically averaged values for the chain backbone and S_1 to S_5 are summarized in Table 1. We can clearly find important differences between the disorder parameter in the region of the lowest excited states (especially S_1) and the disorder of the overall chain; that is, the lowest excited states tend to localize away from geometric defects. Such differences becomes smaller and nonstatistically significant for higher excited states. It should be pointed out that this is only a correlation found by averaging many data between exciton localization and disorder but, at the individual chain level, it is certainly not rare to find low energy excitons in relatively disordered region. This verifies again that pure geometric definition of a chromophore or an exciton is not valid for amorphous polymer systems and where the definitions based on the wave function is certainly advantageous. Another interesting thing is that both λ_f and λ_p characters for the lowest

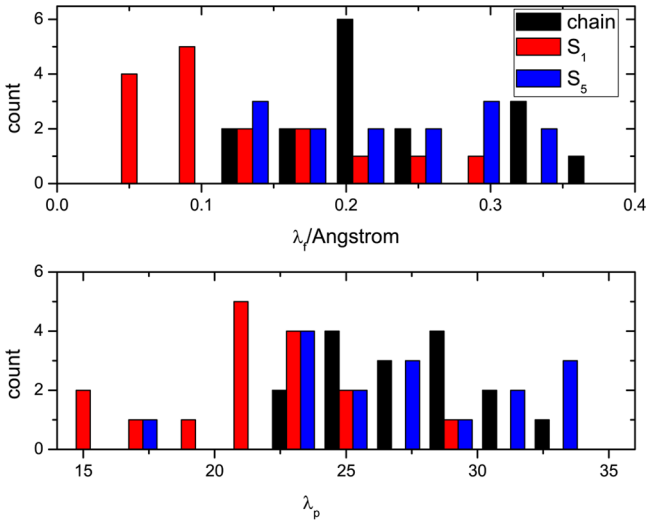

Figure 8. Histogram distribution of chain folding in the top panel and nonplanarity degree in the bottom panel for m20 system at 200 ns.

Table 1. Calculated Average Folding and Nonplanarity Parameters (λ_f and λ_p) for the Lowest 5 Excited States and Their Differences with the Chain Values for m40 System at 200 ns

	chain	S_1	S_2	S_3	S_4	S_5
			λ_f (Å)			
$\langle\lambda_f\rangle$	0.23	0.12	0.21	0.22	0.18	0.25
$\Delta\langle\lambda_f\rangle$	0.00	−0.11	−0.03	−0.01	−0.05	0.02
			λ_p (deg)			
$\langle\lambda_p\rangle$	27.43	21.37	23.96	24.08	24.59	26.80
$\Delta\langle\lambda_p\rangle$	0.00	−6.07	−3.47	−3.36	−2.84	−0.64

excited state S_1 are very similar to those for the highest occupied molecular orbital (HOMO) illustrated in ref 43.

C. Conjugation Length and Charge Transfer Character. Figure 9 shows the histogram distribution of partition ratio (PR) and electron−hole distance (d_{e-h}) for the lowest 5 excited states in 16 individual chains of m20 system at 200 ns, and their

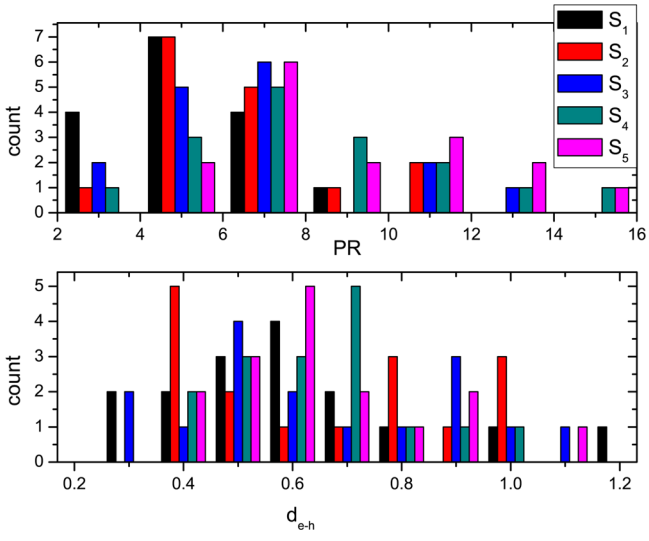

Figure 9. Histogram distribution of partition ratio (PR) in the top panel and electron−hole distance (d_{e-h}) in the bottom panel for the lowest 5 excited states in 16 individual chains of m20 system at 200 ns.

dx.doi.org/10.1021/ct4010799 | J. Chem. Theory Comput. 2014, 10, 1272−1282

averaged values are summarized in Table 2. One may clearly see that lowest three states have similar PR values around 5−7 repeating units and the higher fourth and fifth excited states are more delocalized with PR values around 8−9. Such characteristics have also been shown in Figure 5, where S_1, S_2, and S_3 usually locate at different regions of the chain with very small overlaps between each other while S_4 and S_5 tend to be more delocalized and overlaps with S_1 to S_3 due to the fact that our 20-monomer chain can only locate three lowest excitons at most. Such difference between the delocalization extent of S_4 and S_5 and that of S_1 to S_3 is in accordance with the recent finding that one-electron states at the band edge are usually more localized.[43] Our predicted PR values for lowest excitons (5−7 repeating units) are in quite good agreements with recent reported conjugation length of around 5−6 monomers by absorption spectra experiment at room temperatures for amorphous MEH-PPV in MeTHF[28] and at interface with solids.[75] It should be noticed that such conjugation length will be much dependent on the environmental factors. Low temperature experiment for aggregated MEH-PPV systems gave much larger PR values of around 10−17 repeating units.[28,76] From Table 2, we may also find that the CT characters for the excitons with lowest excitation energies are not strong, d_{e-h} being only around 0.6−0.8 Å. Such small d_{e-h} values mean that lowest excitations in amorphous MEH-PPV polymers are local excitations and charge-transfer excited states will not emerge at low-energy windows for such polymer systems. The very similar d_{e-h} values for the lowest 5 excited states, which determine the binding energy of the exciton,[24] is to a large extent not dependent on the delocalization extent (PR value) of the exciton. This finding apparently disagrees with the finding by Beljonne et al.[48] that CT character may vary evidently for different lowest excited states in interacting MEH-PPV chains. The discrepancy comes possibly from their overestimation of CT percentage for $\pi \rightarrow \pi^*$ excitations. Their reported CT percentage values are even as high as 30−50% for lowest $\pi \rightarrow \pi^*$ excitations in MEH-PPV, which are certainly not CT states. Actually, recent theoretical analysis has noticed such "charge-transfer excitations in disguise" problem for $\pi \rightarrow \pi^*$ excitations in large conjugated systems and attributed it to the small spatial overlap between auxiliary orbitals, which were obtained from original molecular orbitals via a unitary transformation.[77] Such "charge-transfer excitations in disguise" are also considered as the reason for the well-known failure of TDDFT with conventional functionals in describing $\pi \rightarrow \pi^*$ excitations of large conjugated systems. Therefore, we used d_{e-h} instead of widely used CT percentage as the indicator of CT character for large conjugated systems of MEH-PPV in this work. In fact, the exciton of a polymer chain was suggested to be described by two independent particles, that is, a relative particle characterizing the electron−hole separation and a center-of-mass particle characterizing the exciton delocalization.[24] Our results support such a description and show that the size of the relative particle (electron−hole separation) is nearly invariant for all lowest electronic excited states while the size of the center-of-mass particle (exciton delocalization) will get increased for the higher excited states.

Table 2. Calculated Averaged Partition Ratio (PR) and Electron-Hole Distance (d_{e-h}) for the Lowest 5 Excited States in 16 Individual Chains of m20 System at 200 ns

	S_1	S_2	S_3	S_4	S_5
⟨PR⟩	5.22	6.49	6.81	8.12	9.04
$\langle d_{e-h} \rangle$ (Å)	0.66	0.72	0.75	0.72	0.74

D. Interchain Excitonic Coupling. Up to now, our results are based on individual chain calculations with the assumption that the interchain excitonic couplings are neglectable in amorphous polymer systems (or, equivalently, that can be considered as small perturbations). Our discussion about the effect of surrounding electrostatic environment in the earlier part has shown that the influence of other chains on the electronic excited states of one chain is quite small and can be neglected. Here, we further evaluated the interchain excitonic couplings by the distributed monopole approximation[72] (see eq 8) for chain pairs of m20 at 200 ns. For each chain pair under consideration, we evaluated the 3 × 3 couplings between the lowest 3 excited states of each chain. Due to the large number of chain pairs, we sorted them into three different groups according to their closest interatomic distance (r_{min}): r_{min}< 0.5 nm, 0.5 nm ≤r_{min}< 3.0 nm, and 3.0 nm ≤r_{min}< 6.0 nm. Figure 10 shows the histogram distribution of $|J_{ij}^{\alpha\beta}|$ for these three groups. For close pairs with r_{min}< 0.5 nm, it is found that most couplings are less than 10 meV while there are also a few cases with values up to 20 meV but only very rare cases with values larger than 20 meV. Such small magnitude verifies again that excited state properties based on single chain calculations can be taken as good approximations as those for the bulk amorphous polymer systems. For medium separated chain pairs with 0.5 nm ≤r_{min}< 3.0 nm, the couplings with values up to 10 meV are noticeable while the couplings larger than 10 meV are quite few. However, such couplings with magnitudes up to 10 meV should be enough to make such medium-range exciton hopping feasible. This is in accordance with recent exciton dynamics study of PPV based on empirical Frenkel-Holstein model, which predicted an average exciton hopping distance around 3 nm.[22] In contrast to the close or medium separated chain pairs, the long-range separated pairs with 3.0 nm ≤ r_{min}< 6.0 nm have much smaller excitonic couplings, most of which are smaller than 5 meV, implying that the possibility to have long-range exciton hopping is low. Such calculation provides the means to estimate the decrease of the interchain excitonic coupling with the distance between excitons, which can be used

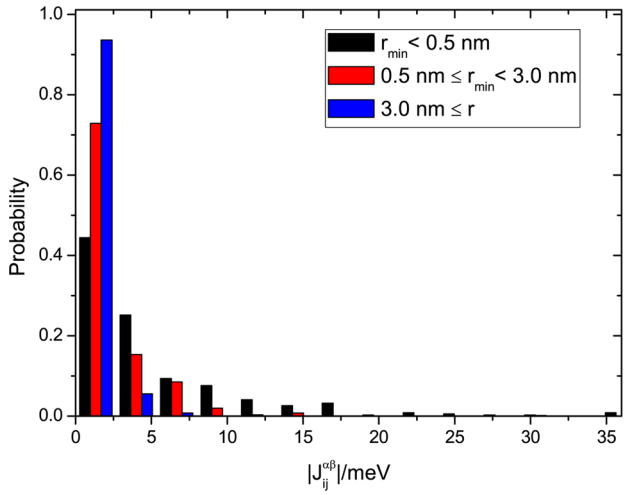

Figure 10. Histogram distribution of $|J_{ij}^{\alpha\beta}|$ for chain pairs of m20 at 200 ns.

to construct a model for exciton transport in amorphous polymers.

E. Dependence of the Excited States on Time Evolved Polymer Chain Conformations. With the above information that excitons with lowest vertical excitation energies are LEGS and the interchain excitonic couplings do not influence the electronic structure of a single chain too much, now we turn our attentions to the dependence of the excited states on time evolved polymer chain conformations. The monomer contributions to the lowest excited state S_1 for three representative chains of m20 system in four different timesteps is shown Figure 11. MEH-PPV is below its glass transition temperature

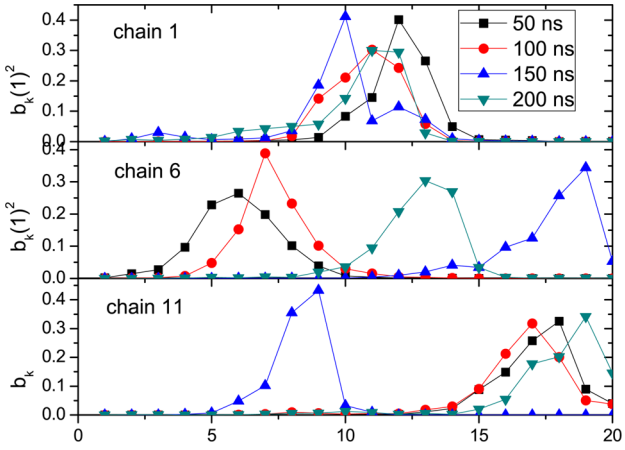

Figure 11. Variation of monomer contributions to the lowest excited state S_1 at different room temperature snapshots for three representative chains of m20 system.

at 300 K, and expectedly, the overall chain conformation is rather stationary over many tens of nanoseconds with only modest geometric fluctuations observed.[43] However, we can find from Figure 11 that the wave function of S_1 may change significantly for both the centroid position and the shape with time. This is partly due to the variation of the torsional disorder with time that can change the magnitude of intrachain couplings and modulate the excitation energy and shape. Very large changes of exciton centroid are instead due to an altered energy ordering of the excitons induced by the fluctuation of the local exciton energy. A previous study[43] also observed similar shape variation phenomenon for DOS and the swap of different molecular orbitals. Nevertheless, it should be emphasized that the varied wave function of lowest excited states preserves the characteristics of LEGS, nodeless localization with PR around 5−6 monomers and very small overlaps with other LEGSs. This indicates that time evolved conformations of the polymer chains may affect the shapes and the energetic order for several lowest excited states but will not affect the nature of excitons. Moreover, these conformational changes are slow with respect to the exciton dynamics and our analysis based on only one snapshot can still give reliable quantitative information for the fundamental characters of the electronic excited states in amorphous polymer materials.

F. Effect of Chain Size and Number of Excited States Included. Before the end of this paper, we would like to show that the chain size does not affect the nature of the electronic excitations in amorphous MEH-PPV if we have incorporated an oligomer composed of 20 monomers. Figure 12 shows the electronic absorption spectra for both m20 and m40 systems at

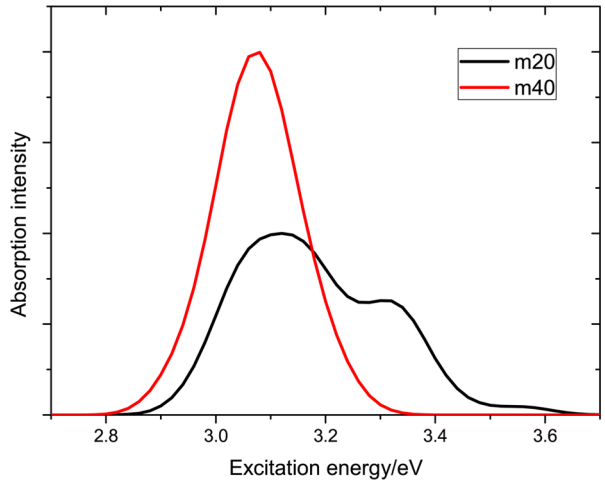

Figure 12. Electronic absorption spectra for both m20 and m40 systems at 200 ns by ωB97X-D/3-21g calculations for lowest three singlet excitations.

200 ns by ωB97X-D/3-21g calculations for lowest three singlet excitations. One may notice that the main peak positions are quite close for m20 and m40, but there is a remarkable shoulder for m20. In some very distorted m20 chains, it is impossible to locate three LEGSs whose typical width is about 5−7 monomers and accordingly higher energy excitations emerges. Such situations hardly occur in m40 due to the doubled size of the chain if we only calculate the lowest three singlet excitations. Therefore, the average transition energies ΔE for the lowest two excitations in m20 (3.08 ± 0.01 and 3.21 ± 0.02 eV) are comparable to those of the lowest three excitations in m40 (3.03 ± 0.01, 3.08 ± 0.01, and 3.15 ± 0.01 eV), but ΔE for the S_3 in m20 (3.35 ± 0.02 eV) is distinctively higher and is at the origin of the shoulder for m20 in Figure 12. Essentially, if one is interested in the lowest excited states (or the LEGSs), the description provided by the model m20 is similar to that of the larger model m40. For example, the determined PR values for the lowest three excited states of m40 are 5.36, 6.09, 6.38, in good agreements with those for m20 (5.22, 6.49, 6.81, as shown in Table 2). This also confirms that our model chains are sufficiently large to provide reliable information for the study of the excitons in amorphous polymers with higher molecular weight.

IV. CONCLUSION

In this paper, we performed large scale TDDFT calculations for the electronic excited states in amorphous MEH-PPV systems based on classical MD trajectories to provide useful information for the relevant photovoltaic or electroluminescent polymer-based materials. Detailed tests for the effects of DFT functionals, basis set and chain size as well as the electrostatic background indicate that our computations present reliable first principles results for such large complicated systems. Our major findings can be outlined as follows:

1. We inferred an average conjugation length of ∼5−7 monomers for lowest vertical excitations of amorphous MEH-PPV at room temperature, in agreements with recent experiments.
2. We verified that it is not really possible to define a chromophore in a polymer on the basis of purely geometric "conjugation breaks". Because of the multiple coexisting mechanisms for excitonic couplings including

dx.doi.org/10.1021/ct4010799 | J. Chem. Theory Comput. 2014, 10, 1272−1282

dipole−dipole and superexchange interactions, the chromophores for the lowest vertical excitations tend to deviate from what one could expect by simply considering the geometry of the individual chain. A rigorous definition can be only based on the evaluation of the polymer excited state wave function. We find that generally the lowest energy exciton avoid the more disordered regions of the chain but a large number of exceptions can also be found.

3. We verified that the exciton of a polymer chain can be described by two independent particles, that is, a relative particle characterizing the electron−hole separation and a center-of-mass particle characterizing the exciton delocalization. We found the size of the relative particle (electron−hole separation) is nearly invariant for all lowest excited states while the size of the center-of-mass particle (exciton delocalization) increases for the higher excited states.
4. We found the interchain excitonic couplings for amorphous MEH-PPV are usually smaller than 10 meV suggesting that the transport mechanism across chain can be described by incoherent hopping.

The above findings concerning on the energetic and spatial distribution of excitons as well as their couplings provide useful information for constructing more realistic models for the further exciton dynamics study. The theoretical scheme employed in this paper builds the bridge linking the phenomenological descriptions of excitons in polymers and microscopic modeling for realistic polymers with chemical characteristics and such kind of scheme can be also applied for the theoretical study of other polymer systems in the future.

Finally, we should note that all our TDDFT computations were based on the classical MD trajectories for the electronic ground state of MEH-PPV chains. It means, in principle, the calculated properties for the excited states here can only apply for vertical excitations because we did not include geometry relaxation upon excitation. However, the picture of the excitons in the polymer presented here is expected to remain generally valid, because several other groups[48,52] have found the potential energy surfaces for the electronic ground state and the lowest excited state are very similar for MEH-PPV systems especially when one considers thermal fluctuations.

AUTHOR INFORMATION

Corresponding Authors

*E-mail: haibo@nju.edu.cn.
*E-mail: a.troisi@warwick.ac.uk.

Notes

The authors declare no competing financial interest.

ACKNOWLEDGMENTS

This work is financially supported by the National Natural Science Foundation of China (Grant Nos. 21003072 and 21373109), National Basic Research Program of China (Grant No. 2011CB808604), and the European Research Council. We thank Juan Arago March and William Barford for helpful discussions and we are also grateful to the High Performance Computing Center (HPCC) of Nanjing University for providing the facilities to perform the numerical calculations in this paper on its IBM Blade cluster system.

REFERENCES

(1) Günes, S.; Neugebauer, H.; Sariciftci, N. S. *Chem. Rev.* **2007**, *107*, 1324.
(2) Heeger, A. J. *Chem. Soc. Rev.* **2010**, *39*, 2354.
(3) Zhao, X.; Zhan, X. *Chem. Soc. Rev.* **2011**, *40*, 3728.
(4) Green, M. A.; Emery, K.; Hishikawa, Y.; Warta, W.; Dunlop, E. D. *Prog. Photovoltaics* **2012**, *20*, 606.
(5) He, Z.; Zhong, C.; Su, S.; Xu, M.; Wu, H.; Cao, Y. *Nat. Photon.* **2012**, *6*, 593.
(6) Facchetti, A. *Chem. Mater.* **2010**, *23*, 733.
(7) Chen, H.; Guo, Y.; Yu, G.; Zhao, Y.; Zhang, J.; Gao, D.; Liu, H.; Liu, Y. *Adv. Mater.* **2012**, *24*, 4618.
(8) Noriega, R.; Rivnay, J.; Vandewal, K.; Koch, F. P. V.; Stingelin, N.; Smith, P.; Toney, M. F.; Salleo, A. *Nat. Mater.* **2013**, *12*, 1038.
(9) Peet, J.; Kim, J. Y.; Coates, N. E.; Ma, W. L.; Moses, D.; Heeger, A. J.; Bazan, G. C. *Nat. Mater.* **2007**, *6*, 497.
(10) Kitazawa, D.; Watanabe, N.; Yamamoto, S.; Tsukamoto, J. *Appl. Phys. Lett.* **2009**, *95*, 053701.
(11) Park, S. H.; Roy, A.; Beaupré, S.; Cho, S.; Coates, N.; Moon, J. S.; Moses, D.; Leclerc, M.; Lee, K.; Heeger, A. J. *Nat. Photon.* **2009**, *3*, 297.
(12) Wang, E.; Hou, L.; Wang, Z.; Hellström, S.; Zhang, F.; Inganäs, O.; Andersson, M. R. *Adv. Mater.* **2010**, *22*, 5240.
(13) Yamamoto, S.; Ohkita, H.; Benten, H.; Ito, S.; Yamamoto, S.; Kitazawa, D.; Tsukamoto, J. *J. Phys. Chem. C* **2013**, *117*, 11514.
(14) Ramasesha, S.; Pati, S. K.; Shuai, Z.; Brédas, J.-L. *Adv. Quan. Chem.* **2000**, *38*, 121.
(15) Arkhipov, V. I.; Emelianova, E. V.; Bassler, H. *Phys. Rev. Lett.* **1999**, *82*, 1321.
(16) Shuai, Z.; Beljonne, D.; Silbey, R. J.; Brédas, J.-L. *Phys. Rev. Lett.* **2000**, *84*, 131.
(17) Arkhipov, V. I.; Heremans, P.; Bassler, H. *App. Phys. Lett.* **2003**, *82*, 4605.
(18) Hendry, E.; Schins, J. M.; Candeias, L. P.; Siebbeles, L. D. A.; Bonn, M. *Phys. Rev. Lett.* **2004**, *92*, 196601.
(19) Hennebicq, E.; Pourtois, G.; Scholes, G. D.; Herz, L. M.; Russell, D. M.; Silva, C.; Setayesh, S.; Grimsdale, A. C.; Mullen, K.; Brédas, J.-L.; Beljonne, D. *J. Am. Chem. Soc.* **2005**, *127*, 4744.
(20) Lee, J.; Vandewal, K.; Yost, S. R.; Bahlke, M. E.; Goris, L.; Baldo, M. A.; Manca, J. V.; Van Voorhis, T. *J. Am. Chem. Soc.* **2010**, *132*, 11878.
(21) Jiang, Y.; Peng, Q.; Gao, X.; Shuai, Z.; Niu, Y.; Lin, S. H. *J. Mater. Chem.* **2012**, *22*, 4491.
(22) Tozer, O. R.; Barford, W. *J. Phys. Chem. A* **2012**, *116*, 10310.
(23) Barford, W.; Bittner, E. R.; Ward, A. *J. Phys. Chem. A* **2012**, *116*, 10319.
(24) Barford, W. *J. Phys. Chem. A* **2013**, *117*, 2665.
(25) Grancini, G.; Maiuri, M.; Fazzi, D.; Petrozza, A.; Egelhaaf, H. J.; Brida, D.; Cerullo, G.; Lanzani, G. *Nat. Mater.* **2013**, *12*, 29.
(26) Collini, E.; Scholes, G. D. *Science* **2009**, *323*, 369.
(27) Campbell, I. H.; Hagler, T. W.; Smith, D. L.; Ferraris, J. P. *Phys. Rev. Lett.* **1996**, *76*, 1900.
(28) Köler, A.; Hoffmann, S. T.; Bässler, H. *J. Am. Chem. Soc.* **2012**, *134*, 11594.
(29) Kumar, P.; Mehta, A.; Mahurin, S. M.; Dai, S.; Dadmun, M. D.; Sumpter, B. G.; Barnes, M. D. *Macromolecules* **2004**, *37*, 6132.
(30) DuBay, K. H.; Hall, M. L.; Hughes, T. F.; Wu, C.; Reichman, D. R.; Friesner, R. A. *J. Chem. Theory Comput.* **2012**, *8*, 4556.
(31) Nayyar, I. H.; Batista, E. R.; Tretiak, S.; Saxena, A.; Smith, D. L.; Martin, R. L. *J. Phys. Chem. Lett.* **2011**, *2*, 566.
(32) Nayyar, I. H.; Batista, E. R.; Tretiak, S.; Saxena, A.; Smith, D. L.; Martin, R. L. *J. Chem. Theory Comput.* **2013**, *9*, 1144.
(33) Ko, S.; Hoke, E. T.; Pandey, L.; Hong, S.; Mondal, R.; Risko, C.; Yi, Y.; Noriega, R.; McGehee, M. D.; Brédas, J.-L.; Salleo, A.; Bao, Z. *J. Am. Chem. Soc.* **2012**, *134*, 5222.
(34) Pandey, L.; Doiron, C.; Sears, J. S.; Brédas, J. -L. *Phys. Chem. Chem. Phys.* **2012**, *14*, 14243.
(35) Panda, A. N.; Plasser, F.; Aquino, A. J. A.; Burghardt, I.; Lischka, H. *J. Phys. Chem. A* **2013**, *117*, 2181.

(36) Saha, B.; Ehara, M.; Nakatsuji, H. *J. Phys. Chem. A* **2007**, *111*, 5473.
(37) Granadino-Roldán, J. M.; Vukmirović, N.; Fernández-Gómez, M.; Wang, L.-W. *Phys. Chem. Chem. Phys.* **2011**, *13*, 14500.
(38) Vukmirović, N.; Wang, L.-W. *J. Phys. Chem. B* **2011**, *115*, 1792.
(39) Poelking, C.; Cho, E.; Malafeev, A.; Ivanov, V.; Kremer, K.; Risko, C.; Brédas, J.-L.; Andrienko, D. *J. Phys. Chem. C* **2013**, *117*, 1633.
(40) Ridley, J. E.; Zerner, M. C. *Theor. Chem. Acc.* **1973**, *32*, 111.
(41) Zerner, M. C. In *Reviews of Computational Chemistry*: Lipkowitz, K. B., Boyd, D. B., Eds.; VCH Publishing: New York, 1991; Vol. *2*, pp 313−366.
(42) Cheung, D. L.; McMahon, D. P.; Troisi, A. *J. Am. Chem. Soc.* **2009**, *131*, 11179.
(43) Qin, T.; Troisi, A. *J. Am. Chem. Soc.* **2013**, *135*, 11247.
(44) Barford, W.; Trembath, D. *Phys. Rev. B* **2009**, *80*, 165418.
(45) Barford, W.; Lidzey, D. G.; Makhov, D. V.; Meijer, A. J. H. *J. Chem. Phys.* **2010**, *133*, 044504.
(46) Malyshev, A. V.; Malyshev, V. A. *Phys. Rev. B* **2001**, *63*, 195111.
(47) Makhov, D. V.; Barford, W. *Phys. Rev. B* **2010**, *81*, 165201.
(48) De Leener, C.; Hennebicq, E.; Sancho-Garcia, J.-C.; Beljonne, D. *J. Phys. Chem. B* **2009**, *113*, 1311.
(49) Tretiak, S.; Middleton, C.; Chernyak, V.; Mukamel, S. *J. Phys. Chem. B* **2000**, *104*, 9540.
(50) Muñoz-Losa, A.; Curutchet, C.; Fdez Galván, I.; Mennucci, B. *J. Chem. Phys.* **2008**, *129*, 034104.
(51) Gisslén, L.; Johansson, Å; Stafström, S. *J. Chem. Phys.* **2004**, *121*, 1601.
(52) Sterpone, F.; Rossky, P. J. *J. Phys. Chem. B* **2008**, *112*, 4983.
(53) Bedard-Hearn, M. J.; Sterpone, F.; Rossky, P. J. *J. Phys. Chem. A* **2010**, *114*, 7661.
(54) Nelson, T.; Fernandez-Alberti, S.; Chernyak, V.; Roitberg, A. E.; Tretiak, S. *J. Phys. Chem. B* **2011**, *115*, 5402.
(55) Runge, E.; Gross, E. K. U. *Phys. Rev. Lett.* **1984**, *52*, 997.
(56) Ullrich, C. A. In *Time-Dependent Density-Functional Theory: Concepts and Applications*; Ullrich, C. A., Ed.; Oxford University Press: New York, 2012; Vol. *1*, pp 4−7.
(57) Jorgensen, W. L.; Tirado-Rives, J. *J. Am. Chem. Soc.* **1988**, *110*, 1657.
(58) Allinger, N. L.; Yuh, Y. H.; Lii, J. H. *J. Am. Chem. Soc.* **1989**, *111*, 8551.
(59) Marcon, V.; Raos, G. *J. Phys. Chem. B* **2004**, *108*, 18053.
(60) Moreno, M.; Casalegno, M.; Raos, G.; Meille, S. V.; Po, R. *J. Phys. Chem. B* **2010**, *114*, 1591.
(61) Chai, J. -D.; Head-Gordon, M. *Phys. Chem. Chem. Phys.* **2008**, *10*, 6615.
(62) Becke, A. D. *J. Chem. Phys.* **1993**, *98*, 5648.
(63) Stephens, P. J.; Devlin, F. J.; Chablowski, C. F.; Frisch, M. J. *J. Phys. Chem.* **1994**, *98*, 11623.
(64) Hertwig, R. H.; Koch, W. *Chem. Phys. Lett.* **1997**, *268*, 345.
(65) Yanai, T.; Tew, D.; Handy, N. C. *Chem. Phys. Lett.* **2004**, *393*, 51.
(66) Zhao, Y.; Truhlar, D. G. *Theor. Chem. Acc.* **2008**, *120*, 215.
(67) Bakowies, D.; Thiel, W. *J. Phys. Chem.* **1996**, *100*, 10580.
(68) Neaton, J. B.; Hybertsen, M. S.; Louie, S. G. *Phys. Rev. Lett.* **2006**, *97*, 216405.
(69) Refaely-Abramson, S.; Sharifzadeh, S.; Jain, M.; Baer, R.; Neaton, J. B.; Kronik, L. *Phys. Rev. B* **2013**, *88*, 081204.
(70) Frisch, M. J.; Trucks, G. W.; Schlegel, H. B.; Scuseria, G. E.; Robb, M. A.; Cheeseman, J. R.; Scalmani, G.; Barone, V.; Mennucci, B.; Petersson, G. A.; Nakatsuji, H.; Caricato, M.; Li, X.; Hratchian, H. P.; Izmaylov, A. F.; Bloino, J.; Zheng, G.; Sonnenberg, J. L.; Hada, M.; Ehara, M.; Toyota, K.; Fukuda, R.; Hasegawa, J.; Ishida, M.; Nakajima, T.; Honda, Y.; Kitao, O.; Nakai, H.; Vreven, T.; Montgomery, J. A., Jr.; Peralta, J. E.; Ogliaro, F.; Bearpark, M.; Heyd, J. J.; Brothers, E.; Kudin, K. N.; Staroverov, V. N.; Kobayashi, R.; Normand, J.; Raghavachari, K.; Rendell, A.; Burant, J. C.; Iyengar, S. S.; Tomasi, J.; Cossi, M.; Rega, N.; Millam, N. J.; Klene, M.; Knox, J. E.; Cross, J. B.; Bakken, V.; Adamo, C.; Jaramillo, J.; Gomperts, R.; Stratmann, R. E.; Yazyev, O.; Austin, A. J.; Cammi, R.; Pomelli, C.; Ochterski, J. W.; Martin, R. L.; Morokuma, K.; Zakrzewski, V. G.; Voth, G. A.; Salvador, P.; Dannenberg, J. J.; Dapprich, S.; Daniels, A. D.; Farkas, Ö.; Foresman, J. B.; Ortiz, J. V.; Cioslowski, J.; Fox, D. J. *Gaussian09*, Revision B.01; Gaussian, Inc.: Wallingford, CT, 2009.
(71) Martin, R. L. *J. Chem. Phys.* **2003**, *118*, 4775.
(72) Marguet, S.; Markovitsi, D.; Millié, P.; Sigal, H.; Kumar, S. *J. Phys. Chem. B* **1998**, *102*, 4697.
(73) Park, J. H.; Yu, H. Y.; Park, J. G.; Kim, B.; Lee, S. H.; Olofsson, L.; Persson, S. H. M.; Park, Y. W. *Thin Solid Films* **2001**, *393*, 129.
(74) Adamo, C.; Jacquemin, D. *Chem. Soc. Rev.* **2013**, *42*, 845.
(75) Li, Q.; Hua, R.; Chou, K. C. *J. Phys. Chem. B* **2008**, *112*, 2315.
(76) Barbara, P. F.; Gesquiere, A. J.; Park, S.-J.; Lee, Y. J. *Acc. Chem. Res.* **2005**, *38*, 602.
(77) Kuritz, N.; Stein, T.; Baer, R.; Kronik, L. *J. Chem. Theory Comput.* **2011**, *7*, 2408.